Arch. Metall. Mater. **65** (2020), 4, 1269-1272

DOI: 10.24425/amm.2020.133682

WON JUNE CHOI[1], CHEONWOONG PARK[1], JONGMIN BYUN[2*], YOUNG DO KIM[1*]

FABRICATION OF MOLYBDENUM ALLOY WITH DISTRIBUTED HIGH-ENTROPY ALLOY VIA PRESSURELESS SINTERING

In this study, a molybdenum alloy with dispersed high-entropy particles was fabricated using the powder metallurgy method. The high-entropy powder, composed of Nb, Ta, V, W, and Zr elements with a same atomic fraction, was prepared via high-energy ball milling. Using this powder, an ideal core-shell powder, composed of high-entropy powder as core and Mo powder as shell, was synthesized via the milling and reduction processes. These processes enabled the realization of an ideal microstructure with the high-entropy phase uniformly dispersed in the Mo matrix. The sintered body was successfully fabricated via uniaxial compaction followed by pressureless sintering. The sintered body was analyzed by X-ray diffraction and scanning electron microscope, and the high-entropy phase is uniformly dispersed in the Mo matrix.

Keywords: Molybdenum alloy, High-entropy alloys, Core-shell powder

1. Introduction

Several studies have explored the improvement of energy efficiency since the usage of fossil fuels began. In recent times, with the implementation of various environmental regulations in the world such as the Kyoto protocol, increasing energy efficiency has become essential. Therefore, many studies have been conducted in various fields regarding energy efficiency. For example, the gas turbine, invented in the 1970s, has undergone gradual upgradation for enhancement of its efficiency. In particular, the turbine inlet temperature has been significantly increased with the development of materials that have high strength and outstanding durability [1-3]. Similarly, to increase the operating temperature in various fields, high-temperature materials are required. In other words, it is necessary to develop high-temperature materials that have high melting points and favorable properties.

Molybdenum (Mo) is a typical refractory metal that has a high melting point compared to other metals. It has been widely investigated owing to the rising necessity for high-temperature materials. Pure Mo has a high melting point of approximately 2623°C. However, it has poor oxidation and mechanical properties compared to intermetallic compounds [4-6]. As a result, Mo alloys, composed of an Mo phase and Mo-Si intermetallic compounds phases such as $MoSi_3$ and Mo_5Si_3, have been studied with the aim of improving their mechanical properties and oxidation resistance [7-9]. However, despite the improvement of the mechanical or oxidation properties of Mo alloys, machining this alloy is difficult because of poor ductility of the alloys at room temperature. To solve this problem, it would be desirable to search for phases with sufficient ductility and strength similar to intermetallic compound phases. A high-entropy alloy, defined by Yeh et al. [10], serves as one of the solutions and has been investigated extensively in the last few decades. It is composed of five or more metallic elements of similar composition. This alloy is well known for its outstanding strength and moderate ductility at room and elevated temperatures [11-14]. Recently, research on high-entropy alloys has been conducted based on compositional changes and mechanical properties. However, limited research has been conducted on high-entropy alloys as the dispersoid in metal matrix such as Fe matrix or Mo matrix. In this study, we focus on the possibility of Mo alloys fabrication with dispersed high-entropy phases via the powder metallurgy method. To disperse the high-entropy alloy uniformly, core-shell structured powder which is composed of Mo powder as shell and high-entropy powder as core was synthesized. The green body was fabricated via the uniaxial pressing and was sintered under a H_2 atmosphere. The phase, microstructure, and morphology of powder and sintered body was investigated.

[1] HANYANG UNIVERSITY, DEPARTMENT OF MATERIALS SCIENCE & ENGINEERING, 222 WANGSIMNI-RO, SEONGDONG-GU, SEOUL, REPUBLIC OF KOREA, 04763
[2] SEOUL NATIONAL UNIVERSITY OF SCIENCE & TECHNOLOGY, DEPARTMENT OF MATERIALS SCIENCE & ENGINEERING, 232 GONGNEUNG-RO, NOWON-GU, SEOUL, REPUBLIC OF KOREA, 01811

* Corresponding authors: byun@seoultech.ac.kr, ydkim1@hanyang.ac.kr

2. Experimental

First, Nb (<45 μm, 99.9%, RND Korea), Ta (<45 μm, 99.95%, RND Korea), V (<45 μm, 99.9%, RND Korea), W (<45 μm, 99.9%, RND Korea), and Zr (<45 μm, 99.99%, RND Korea) powders were prepared for the fabrication of high-entropy powders as starting materials. These powders were weighted to have the same atomic ratio (Nb:Ta:V:W:Zr = 1:1:1:1:1, at.%). A total of 100 g powder was placed in a planetary milling jar along with 0.1 wt.% (0.1 g) of stearic acid to prevent agglomeration. Using the planetary ball milling (Retsch, PM400) process, high-energy ball milling was conducted for 30 h at a speed of 200 rpm in an Ar atmosphere. The fabricated high-entropy powder was obtained in a glove box while the inert atmosphere was maintained.

After high-entropy powder fabrication, the MoO_3 (<8 μm, 99.9%, RND Korea) powder was used as the precursor of Mo phase. A nominal composition was set to have a 40% volume ratio for Mo phase and 60% volume ratio for high-entropy phase. MoO_3 and the as-synthesized high-entropy powder were uniformly mixed via another ball milling process. After mixing process, the MoO_3 powder was reduced in an electric furnace at 600°C for 3 h under a H_2 atmosphere. The green bodies were prepared under uniaxial pressure at 300 MPa. They were also sintered in electric furnace at 1400°C for 3 h under a H_2 atmosphere.

A phase analysis was performed through X-ray diffraction (XRD, Rigaku, MiniFlex600) with Cu K_α radiation (0.1542 nm) generated at 40 kV. XRD was also used to examine the formation of high-entropy powder. The microstructures of the powder and sintered body were observed by using the field emission scanning electron microscope (FE-SEM, FEI, Verios G4 UC). We also attempted a quantitative analysis using energy dispersive spectroscopy (EDS, EDAX, Octane Elect EDS System) to identify the distribution of each atom. The hardness is measured via the Vickers hardness tester (Shimadzu, HMV-2)

3. Results and Discussion

The pure starting materials, namely Nb, Ta, V, W and Zr, were ball-milled via planetary ball milling, and the X-ray patterns of the ball-milled powder are shown in Fig. 1. During the initial stage, the different peaks of each starting material could be distinguished easily, and it was confirmed that all the starting materials were pure elements. However, with an increase in the milling time, the intensity of the peaks decreased continuously. Moreover, some of the peaks, such as those for V and Zr, seemingly disappeared after 2 h due to peak broadening. The peaks could barely be distinguished 20 h after milling owing to the low crystallinity. This occurred due to lattice distortion during the alloying process, thus making the formation of high-entropy powder evident. After 30 h of milling, there were no distinguishing peaks of the ball-milled powder. Further, slight peak broadening was noticed due to the decrease in crystalline size.

Another ball-milling process was performed to mix the as-synthesized high-entropy powder and MoO_3 powder, which

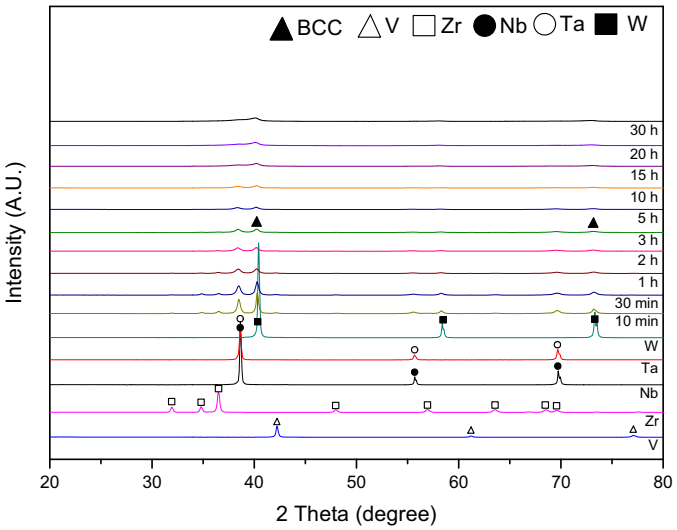

Fig. 1. X-ray diffraction patterns of starting materials and ball-milled powder for up to 30 h under Ar atmosphere

is a precursor of the Mo phase. Further, the mixed powder was heat-treated using an electric furnace; its results are shown in Fig. 2. It is well known that the MoO_3 phase is reduced to the Mo phase when the temperature range is between 450 and 800°C under a H_2 atmosphere [15,16]. The reduction step can be explained using Eqs. (1) and (2).

$$MoO_3(s) + H_2(g) \rightarrow MoO_2(s) + H_2O(g) \quad (1)$$

$$MoO_2(s) + 2H_2(g) \rightarrow Mo(s) + 2H_2O(g) \quad (2)$$

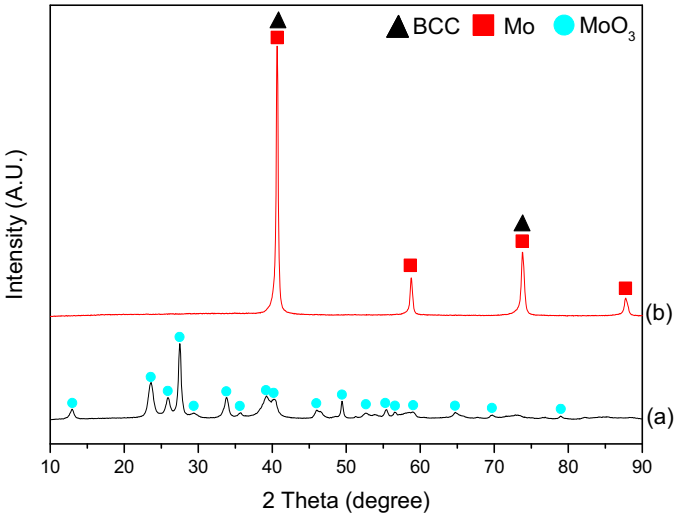

Fig. 2. X-ray diffraction patterns of powder (a) Ball-milled powder with MoO_3 and as-synthesized high-entropy powder and (b) Reduced powder composed of Mo and high-entropy powder

During reduction, gaseous transport phases, such as the $MoO_3(OH)_2$ phase, were produced as an intermediate product. These phases facilitate mass transportation and are called chemical vapor transport (CVT). As a result, nano-sized Mo powder can be fabricated uniformly on the surface of high-entropy powder. As shown in Fig. 2, the MoO_3 phase in the mixing

powder was reduced to the Mo phase in a heat-treated powder. In addition, as shown in Fig. 3, a core-shell structured powder composed of a high-entropy powder as the core and Mo powder as the shell was created through the reduction process. This powder can serve as an ideal microstructure, where the high-entropy phase is uniformly dispersed in the Mo matrix phase. Further, the sintering temperature can be lower owing to nano-sized Mo powder at the shell. It can inhibit the atomic diffusion of high-entropy elements which is more active at elevated temperature. In Fig. 3, at the center of the powder, five elements that were used for high-entropy powder were detected uniformly, and the results of their quantitative analysis are listed in Table 1. A small amount of Mo element was also found due to the interference of the shell regions. In addition, Mo element was detected in most of the shell area. As a result, it is confirmed that nano-sized Mo particles, which were reduced from the MoO_3 phase, surrounded the high-entropy powder uniformly.

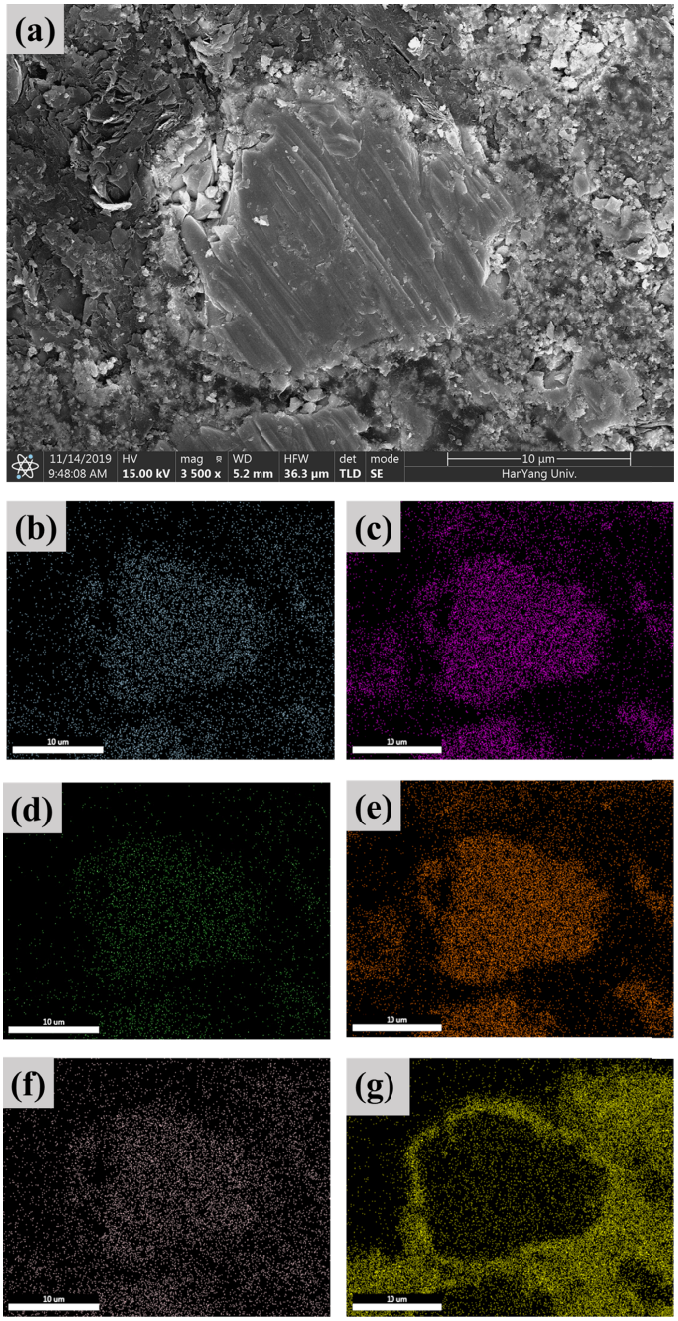

Fig. 3. (a) Cross-sectional SEM image of reduced powder. SEM-EDS mapping analysis of each element; (b) Nb, (c) Ta, (d) V, (e) W, (f) Zr, and (g) Mo

TABLE 1

Atomic percent of each element in the powder and sintered body

Sample		Composition (at.%)					
		Nb	Ta	V	W	Zr	Mo
Powder	Core	17.4	20.2	21.2	14.9	22.6	3.8
	Edge	0.6	1.2	2.3	0.4	2.9	92.6
Sintered body	Dispersoid	11.3	21.7	24.1	19.5	23.4	—
	Matrix	6.9	1.6	6.1	0.6	0.3	84.4

With the use of the core-shell powder, the sintered body was fabricated via the pressing process followed by the sintering process; its SEM image is shown in Fig. 4. As shown in Fig. 4, high-entropy powder, which is whitish gray and has a particle size of 5-10 µm, was dispersed uniformly in the Mo matrix. Several pores were observed near the high-entropy powder. However, the pores were barely observed in the Mo matrix. It was assumed that sintering is not complete due to the large high-entropy powder. This phenomenon is caused by the difference in driving force according to the particle size. To determine the distribution of each element, SEM-EDS analysis was conducted; its results are depicted in Fig. 4 and listed in Table 1. The matrix region is primarily composed of Mo element, whereas elements of the dispersoid region are similar to those of high-entropy powder. However, some elements, such as V and Nb, are diffused into the Mo matrix region with amounts of approximately 6 at.%, as listed in Table 1. This phenomenon might occur during the sintering process, which progresses at 1400°C for 5 h. It is assumed that V and Nb have a relatively high diffusivity compared to the other elements such as Zr, Ta, and W. This result corresponds to that of the SEM-EDS mapping analysis. In Figs. 4(a) and 4(c), V and Nb elements are detected not only in the regions of the high-entropy phase but also in the regions of the Mo matrix. On the other hand, Zr, Ta, and W have a lower diffusivity in the Mo matrix. We measured the hardness of Mo alloys with dispersed high-entropy alloys via the Vickers hardness test. The hardness value of this alloy is 1.547 ± 0.101 GPa, and this value is similar to that of pure Mo with about 1.530 GPa. This result is reasonable when it considers the hardness value of various high-entropy alloys from 1.471 GPa to 11.77GPa, depending on the element, composition, and fabrication method [17,18]. It assumed that hardness of high-entropy alloys is close to that or pure Mo alloy.

4. Conclusions

In this study, high-entropy powder composed of Nb, Ta, V, W, and Zr elements was fabricated via high-energy ball milling. Further, another ball milling process was conducted on high-

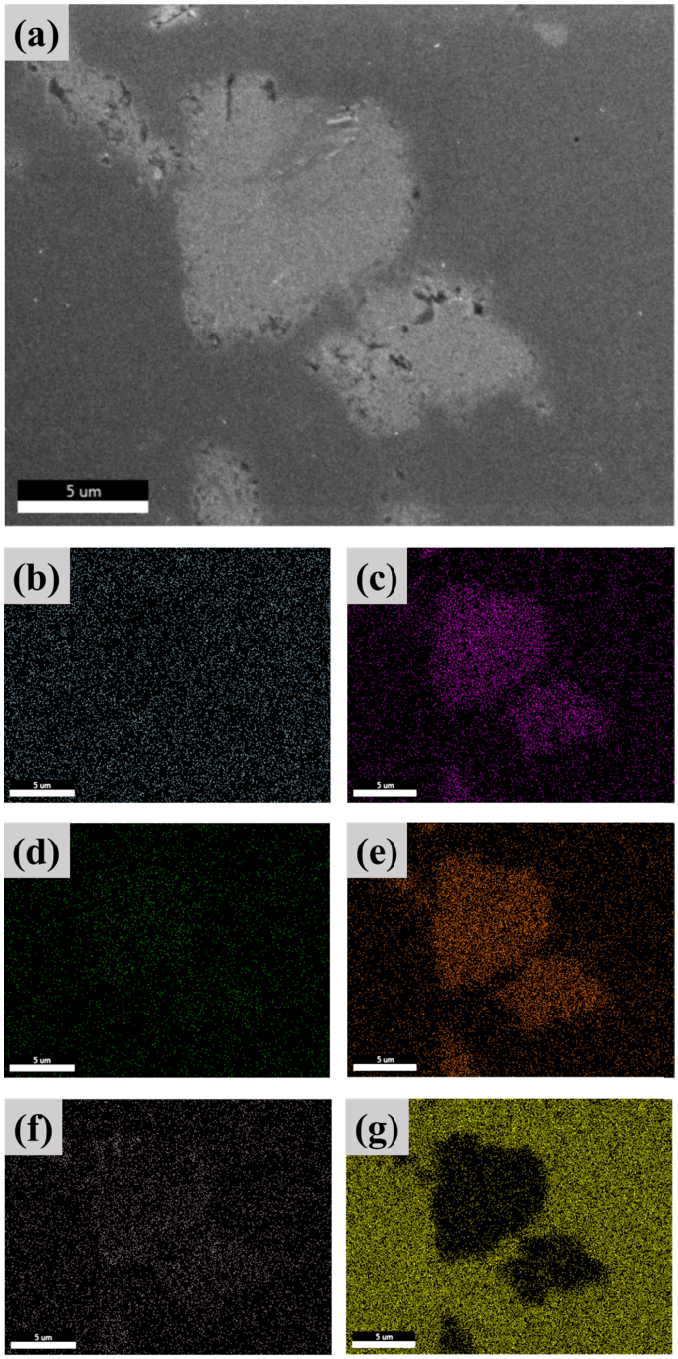

Fig. 4. (a) SEM image of sintered body. SEM-EDS mapping analysis of each element; (b) Nb, (c) Ta, (d) V, (e) W, (f) Zr, and (g) Mo

entropy powder to mix the MoO_3 and high-entropy powders. This powder was heat-treated under a H_2 atmosphere to reduce the MoO_3 phases to the Mo phase. This led to the formation of an ideal core-shell powder, composed of high-entropy powder in the core and Mo powder in the shell. The sintered body was fabricated using the core-shell powder via the pressureless sintering process. The high-entropy phase was well dispersed in the Mo matrix, while minimal amounts of certain elements, such as V and Nb, were diffused into the Mo matrix. The Vickers hardness value of sintered body is 1.547 ± 0.101 GPa. In a future study, the mechanical properties and microstructure of sintered bodies will be investigated to determine the effect of a high-entropy phase as a dispersoid compared to pure Mo alloy.

Acknowledgments

This research was supported by a Basic Science Research Program through the National Research Foundation of Korea (NRF) funded by the Ministry of Education (NRF-2018R1D1A1A09084113), and This work was supported by the Human Resources Program in Energy Technology of the Korea Institute of Energy Technology Evaluation and Planning (KETEP), granted financial resource from the Ministry of Trade, Industry & Energy, Republic of Korea. (No. 20174030201750)

REFERENCES

[1] J.J. Kruzic, J.H. Schneibel, R.O. Ritchie, Metall. Mater. Trans. A **36A** (9), 2393-2402 (2005).
[2] A. Lange, R. Braun, Corros. Sci. **84**, 74-84 (2014).
[3] M.R. Middlemas, J.K. Cochran, JOM **62** (10), 20-24 (2010).
[4] D. Sturm, M. Heilmaier, J.H. Schneibel, P. Jéhanno, B. Skrotzki, H. Saage, Mater. Sci. Eng., A **463** (1-2), 107-114 (2007).
[5] J. Wadsworth, T.G. Nieh, J.J. Stephens, Int. Mater. Rev. **33** (1), 131-150 (1988).
[6] B.V. Cockeram, Metall. Mater. Trans. A **40** (12), 2843-2860 (2009).
[7] X. Tan, Y.J. Tan, J. Liu, T. Jin, Met. Mater. Int. **21** (2), 222-226 (2015).
[8] Y. Yuan, Z.H. Zhong, Z.S. Yu, H.F. Yin, Y.Y. Dang, X.B. Zhao, Z. Yang, J.T. Lu, J.B. Yan, Y. Gu, Met. Mater. Int. **21** (4), 659-665 (2015).
[9] H.U. Hong, K.M. Park, H.S. Kim, I.S. Kim, B.G. Choi, C.Y. Jo, T.K. Woo, J.H. Lee, Korean J. Met. Mater. **51** (3), 159-168 (2013).
[10] J.W. Yeh, S.K. Chen, S.J. Lin, J.Y. Gan, T.S. Chin, T.T. Shun, C.H. Tsau, S.Y. Chang, Adv. Eng. Mater. **6** (5), 299-303 (2004).
[11] O.N. Senkov, G.B. Wilks, J.M. Scott, D.B. Miracle, Intermetallics **19** (5), 698-706 (2011).
[12] H. Kim, S. Nam, A. Roh, M. Son, M.H. Ham, J.H. Kim, H. Choi, Int. J. Refract. Met. Hard Mater. **80**, 286-291 (2019).
[13] B. Gludovatz, A. Hohenwarter, D. Catoor, E.H. Chang, E.P. George, R.O. Ritchie, Science **345** (6201), 1153-1158 (2014).
[14] D.B. Miracle, O.N. Senkov, Acta Mater. **122**, 448-511 (2017).
[15] Y.J. Lee, Y.I. Seo, S.H. Kim, D.G. Kim, Y.D. Kim, Appl. Phys. A**97**, 237-241 (2009).
[16] W.V. Schulmeyer, H.M. Ortner, Int. J. Refract. Met. Hard Mater. **20**, 261-269 (2002).
[17] B. Schuh, F. Mendez-Martin, B. Volker, E. George, H. Clemens, R. Pippan, A. Hohenwarter, Acta Mater. **96**, 258-268 (2015).
[18] H. Zhang, Y. He, Y. Pan, Scr. Mater. **69**, 342-345 (2013).